

The effect of the environment on the structure, morphology and star-formation history of intermediate-redshift galaxies

Kshitija Kelkar^{1*}, Meghan E. Gray¹, Alfonso Aragón-Salamanca¹,
Gregory Rudnick², Bo Milvang-Jensen³, Pascale Jablonka⁴, Tim Schrabback⁵

¹*School of Physics & Astronomy, University of Nottingham, Nottingham NG7 2RD, UK*

²*Department of Physics and Astronomy, University of Kansas, KS 66045-7582*

³*Dark Cosmology Centre, Niels Bohr Institute, University of Copenhagen, Juliane Maries Vej 30, 2100, Copenhagen, Denmark*

⁴*Laboratoire d'Astrophysique, cole Polytechnique Fdrale de Lausanne (EPFL), Observatoire de Sauverny, 1290, Versoix, Switzerland; GEPI, Observatoire de Paris, CNRS UMR 8111, Universit Paris Diderot, 92125, Meudon Cedex, France*

⁵*Argelander Institut fuer Astronomie, Auf dem Huegel 71, D-53121 Bonn, Germany*

Accepted xxx. Received xxx; in original form xxx

ABSTRACT

With the aim of understanding the effect of the environment on the star formation history and morphological transformation of galaxies, we present a detailed analysis of the colour, morphology and internal structure of cluster and field galaxies at $0.4 \leq z \leq 0.8$. We use *HST* data for over 500 galaxies from the ESO Distant Cluster Survey (EDisCS) to quantify how the galaxies' light distribution deviate from symmetric smooth profiles. We visually inspect the galaxies' images to identify the likely causes for such deviations. We find that the residual flux fraction (*RF*), which measures the fractional contribution to the galaxy light of the residuals left after subtracting a symmetric and smooth model, is very sensitive to the degree of structural disturbance but not the causes of such disturbance. On the other hand, the asymmetry of these residuals (A_{res}) is more sensitive to the causes of the disturbance, with merging galaxies having the highest values of A_{res} . Using these quantitative parameters we find that, at a fixed morphology, cluster and field galaxies show statistically similar degrees of disturbance. However, there is a higher fraction of symmetric and passive spirals in the cluster than in the field. These galaxies have smoother light distributions than their star-forming counterparts. We also find that while almost all field and cluster S0s appear undisturbed, there is a relatively small population of star-forming S0s in clusters but not in the field. These findings are consistent with relatively gentle environmental processes acting on galaxies infalling onto clusters.

Key words: galaxies: clusters: general–galaxies: elliptical and lenticular, cD–galaxies: evolution–galaxies: spiral–galaxies: interactions

1 INTRODUCTION

Galaxy clusters represent an excellent agglomeration of galaxy populations undergoing changes in several observable galaxy properties, some of which are attributed to the diversity of environments that the galaxies experience. One of the earliest suggestions that environment may play a role in transforming galaxy properties is the well established morphology–density relation (Dressler 1980, 1984): high density environments are observed to contain higher fractions of galaxies with early-type morphologies than the field. The question of precisely to what extent, and by what physical processes, the environment leaves an imprint on morphology as well as other observable properties (e.g. colour, star formation, internal structure) is still largely undetermined.

Evidence of global transformations happening over look-back time is given by the increasing fraction of spiral galaxies in clusters till $z \sim 0.5$ (Dressler et al. 1997; Fasano et al. 2000; Desai et al. 2007) and the fact that high- z clusters are found to contain more star-forming galaxies as compared to present-day clusters (Butcher & Oemler 1984; Poggianti et al. 2006). In addition to the morphology–density relation, it is widely observed that the specific star-formation rate declines towards dense local environments (Hashimoto et al. 1998; Lewis et al. 2002; Kauffmann et al. 2004; Gray et al. 2004; Balogh et al. 2007). Higher fractions of passive or quiescent galaxies are found in dense environments, both in the local Universe (Baldry et al. 2006; van den Bosch et al. 2008; Gavazzi et al. 2010; Haines et al. 2013) and out to $z \sim 2$ (Poggianti et al. 1999; Cooper et al. 2012; Sobral et al. 2011; Quadri et al. 2012; Woo et al. 2013; Kovač et al. 2014).

Some environmental segregation in the galaxies' properties is

* E-mail: ppxk1@nottingham.ac.uk (KK)

naturally expected: hierarchical models of structure formation predict that the densest regions will collapse at earlier times, forming the cores of clusters. The cluster galaxies at a given epoch will, therefore, be more evolved than the average field galaxy (De Lucia, Kauffmann & White 2004). Further, the decline in global star-formation rate with redshift (Madau 1997; Ferguson, Dickinson & Williams 2000) will result in fewer star-forming field galaxies being accreted onto clusters at later times. However, as the clusters assemble and evolve, the accreting galaxies are also subjected to various interactions with other galaxies and the wider group or cluster environment.

These physical processes will impact the galaxies in different ways, affecting both star-formation rates and stellar distributions. Strong gravitational interactions such as mergers and strong tidal interactions (Barnes & Hernquist 1992, 1996), are efficient in altering galaxy structure as well as triggering star formation. Indeed, it has been observed that most starbursts or galaxies with very high star formation display merger signatures, irrespective of redshift (Duc et al. 1997; Elbaz & Cesarsky 2003). Recent studies like Kartaltepe et al. (2012), however, show that extreme star-forming galaxies since $z \sim 2$ are comprised of a mix regular morphology galaxies and galaxies showing early stages of interaction/ongoing mergers. Tidal interactions or harassment lead to stripping of outer material from the galaxy under the impact of high-speed encounters, resulting in temporary enhancement of star formation (Boquien et al. 2009; Moore et al. 1996).

While gravitational interactions may redistribute the stellar content of the galaxy or trigger bursts of star formation, gaseous processes also influence the star formation rate. With $\sim 10\%$ of the total mass of the cluster consisting of hot intracluster medium (ICM), infalling galaxies may undergo loss of their cold disk gas through ram-pressure stripping (Gunn & Gott 1972) or hot gaseous halo through starvation (Larson, Tinsley & Caldwell 1980). Low-redshift observational studies have shown evidence of stripping of the material from galaxies in cluster environments in the form of ‘jellyfish’ galaxies (Kenney, van Gorkom & Vollmer 2004; Merluzzi et al. 2013; Fumagalli et al. 2014; Jaffé et al. 2015).

Several types of transition objects have been identified that represent populations of galaxies in the process of having their star formation shut down. For example, ‘post-starburst’ or ‘k+a’, galaxies make up a significant fraction of intermediate to high- z clusters, while being rare at $z = 0$. Further, the strong correlation between cluster velocity dispersion and ‘k+a’ fraction suggests a possibility of interactions with the ICM being responsible for the eventually turning them passive (Poggianti et al. 2009), though it may not be the dominant process for the transformation (De Lucia et al. 2009). Structurally, this could be related to the transformation of star-forming spiral galaxies into lenticular galaxies, as discussed by Dressler et al. (1997) and Poggianti et al. (1999), further corroborated by the lack of blue lenticulars in clusters (Jaffé et al. 2011). Indeed, Gallazzi et al. (2009) and Wolf et al. (2009) found a cluster-specific population of smooth spiral galaxies with suppressed star formation in the STAGES multiple-cluster system (Gray et al. 2009). Analysis of rotation curves by Bösch et al. (2013) confirmed that these same objects contain kinematically disturbed gas while remaining optically symmetric. It is clear that for these smooth passive spirals, gas processes such as starvation and ram-pressure stripping (Haines et al. 2013) are shutting down star formation without simultaneous wide-scale redistribution of their stellar material.

When attempting to understand the connections between changes in star formation and structure, one key challenge is to

identify the *cause* of structural disturbances. There have been many methods developed for identifying and analysing specific gravitational interactions such as mergers (which are capable of leaving prominent signatures observable over long timescales). These approaches often involve measuring the structural properties in galaxy images, like the CAS (Conselice 2003) or Gini- M_{20} (Lotz, Primack & Madau 2004) systems. Other approaches include using multimode (M), intensity (I), and deviation (D) statistics to identify galaxies which are likely mergers (Freeman et al. 2013), or analysing the residual light remaining when a smooth profile is removed (Hoyos et al. 2012). Each of these methods is found to be sensitive to different stages or types of interaction, for example, the CAS criteria tends to pick out all major mergers, whereas the Gini/ M_{20} measures both minor and major mergers (Lotz et al. 2008, 2010). However, none of these methods are able to produce a complete and uncontaminated sample of galaxy interactions or structural disturbances, highlighting the complexity of quantifying galaxy structure and interpreting it. Furthermore, these methods give no insight into the physical causes of any asymmetries (reflecting internal brightness fluctuations, or evidence of external gravitational influences), so visual interpretation of images is invaluable.

In this paper, we seek to explore the interconnected relationships between galaxy morphology, star formation properties, and environment, while introducing additional information about the irregularities in the stellar distribution, as well as interpretations of the probable cause of any disturbances. We focus on galaxies in cluster and field environments at intermediate redshifts within $0.4 < z < 0.8$, using the ESO Distant Cluster Survey (EDisCS). We aim to quantify galaxy structure using quantitative analysis of galaxy images (complementing previous work on on bulge/disk decompositions by Simard et al. 2009), as well incorporating visually determined information from galaxies. We further study the correlations of galaxy structure with the observed photometric properties of galaxies and global environment (this paper) and eventually linking them to the star formation history of galaxies and the local environment (Kelkar et al. 2017, in prep).

This paper is structured as follows: Sections 2 and 3 describe the data, the sample selection, and the methodology used when defining the environment and defining galaxy structure. Sections 4, 5, and 6 analyse and discuss the galaxies’ structure, photometric properties and environment. Finally, in Section 7 we present a discussion of our results and conclusions. Throughout this paper, we use the standard Λ CDM Cosmology with $h_0 = 0.7$, $\Omega_\Lambda = 0.7$ and $\Omega_m = 0.3$. When relevant, we use a Kroupa IMF (Kroupa 2001) and AB magnitudes¹.

2 DATA

The data analysed in this paper was described in detail in Kelkar et al. (2015). To avoid repetition, we only provide here a brief summary of the most relevant information. We refer the interested reader to that paper.

Our data originate from the ESO Distant Cluster Survey (EDisCS; White et al. 2005), which studied 20 fields containing galaxy clusters from the Las Campanas Distant Cluster Survey (Gonzalez et al. 2001) in the redshift range $0.4 < z < 1$. Optical imaging in the V , R and I bands was obtained with FORS2 on

¹ The original EDisCS papers published Vega magnitudes. These were converted into the AB system by Rudnick et al. (2017, submitted).

Table 1. Summary of the cluster sample properties (including secondary clusters identified along the line-of-sight, cf. §2.1), sorted according to cluster halo mass. Columns 1–5 contain the cluster ID, cluster redshift, cluster velocity dispersion, cluster halo mass (calculated following Finn et al. 2005) and the number of spectroscopically confirmed cluster members (Halliday et al. 2004; Milvang-Jensen et al. 2008).

Cluster	z_{cl}	σ_{cl} (km s^{-1})	$\log M_{\text{cl}}$ (M_{\odot})	No. of spec. members
<i>Clusters</i>				
cl1232–1250	0.5414	1080^{+119}_{-89}	15.21	54
cl1216–1201	0.7943	1018^{+73}_{-77}	15.06	67
cl1138–1133	0.4796	732^{+72}_{-76}	14.72	49
cl1354–1230	0.7620	648^{+105}_{-110}	14.48	22
cl1054–1146	0.6972	589^{+78}_{-70}	14.38	49
cl1227–1138	0.6357	574^{+72}_{-75}	14.36	22
cl1138–1133a	0.4548	542^{+63}_{-71}	14.33	14
cl1037–1243a	0.4252	537^{+46}_{-48}	14.33	43
cl1054–1245	0.7498	504^{+113}_{-65}	14.16	36
cl1040–1155	0.7043	418^{+55}_{-46}	13.93	30
cl1227–1138a	0.5826	432^{+225}_{-81}	13.69	11
<i>Groups</i>				
cl1103–1245a	0.6261	336^{+36}_{-40}	13.66	15
cl1037–1243	0.5783	319^{+53}_{-52}	13.61	16
cl1103–1245b	0.7031	252^{+65}_{-85}	13.27	11

the ESO Very Large Telescope (VLT; White et al. 2005). Near-IR J and K_s photometry from SOFI at the 3.5 m New Technology Telescope (NTT) is also available (Rudnick et al. 2009). Spectroscopy with FORS2/VLT was obtained for an effectively I -band-selected sample of galaxies with redshifts at or near the cluster redshifts (Halliday et al. 2004; Milvang-Jensen et al. 2008).

In addition, the cluster fields studied here also have *HST* I -band ($F814W$) imaging obtained with the ACS camera (Desai et al. 2007). A total of five pointings were taken in each field, four adjacent one-orbit pointings covering $6.5' \times 6.5'$ (approximately the field of the VLT optical images) and an additional four-orbit pointing covering the central $3.3' \times 3.3'$ region of each cluster. Mosaic stacks that encompass all ACS tiles for a given cluster were created employing `MultiDrizzle` (Koekemoer et al. 2003), and scripts for optimised image registration and weighting as detailed in Schrabback et al. (2010). The work presented in this paper exploits the *HST* imaging to carry out the structural analysis of the galaxies. Table 1 gives a summary of the properties of the cluster sample.

Other follow-up data for these clusters include *Spitzer* IRAC ($3 - 8\mu\text{m}$) and MIPS ($24\mu\text{m}$) imaging, $\text{H}\alpha$ narrow-band imaging for three of the fields (Finn et al. 2005), and *XMM-Newton/EPIC* X-ray observations for a subset of the clusters (Johnson et al. 2006).

HST-based visual galaxy morphologies were published by Desai et al. (2007). For the purposes of this study, we have collapsed the fine morphological classes given by the original catalogue into four broad bins: ellipticals, lenticulars, spirals, and irregulars.

2.1 Environment definition

We separate the sample by global environment based on spectroscopic cluster membership. A galaxy is considered a member of a cluster if its spectroscopic redshift lies within $\pm 3\sigma_{\text{cl}}$ from the average cluster redshift z_{cl} (Milvang-Jensen et al. 2008; Halliday et al. 2004). All the galaxies that do not satisfy this criterion are considered to be in the field sample. Although the redshift distribution

Table 2. Details of the full spectroscopic sample and subsample, divided by environment and morphology. The subsample has a stellar mass-completeness of $\log M_*/M_{\odot} = 10.6$.

Spectroscopic sample		E	S0	Sp	Irr	Total
Cluster	All	104	46	195	16	361
	Mass-complete	65	30	95	4	194
Field	All	31	9	91	20	151
	Mass-complete	15	6	35	1	57

of cluster and field galaxies are very similar, to avoid potential biases we only consider field galaxies whose redshifts are contained within the redshift range spanned by the clusters (with a z tolerance of ± 0.05 at each end, i.e., from the lowest and the highest cluster redshift in our sample).

Some of the EDisCS fields contain secondary clusters in addition to the main ones (White et al. 2005; Milvang-Jensen et al. 2008). Members of these secondary clusters are, for consistency, also included in the cluster sample. These secondary clusters are denoted in Table 1 with ‘a’ or ‘b’ following the main cluster ID. Poggianti et al. (2009) classified these secondary structures into clusters and groups. Structures with $\sigma_{\text{cl}} > 400 \text{ km s}^{-1}$ were classed as ‘clusters’, while structures with $160 < \sigma_{\text{cl}} < 400 \text{ km s}^{-1}$ and at least 8 spectroscopic members were classed as ‘groups’. In this paper, the global environment of the galaxies is defined based on their cluster membership irrespective of the host cluster/group identification.

2.2 Sample selection

In what follows, we will use both the whole spectroscopic sample defined in Section 2.1 (to maximise the number of galaxies) and a mass-complete subsample containing 265 galaxies with a stellar mass completeness limit of $\log M_*/M_{\odot} = 10.6$ (Vulcani et al. 2010). The mass-complete subsample will be used to ensure that no mass-related biases affect our conclusions.

Note that both samples contain only galaxies whose spectra have a S/N ratio in the continuum that is larger than 2. This ensures not only the reliability of the redshifts, but also a reasonable quality in the measurements of spectral features such as the 4000\AA break, the $[\text{OII}]\lambda 3727$ emission line, and several strong Balmer absorption lines. These spectral features are analysed in Kelkar et al. (2017, in prep) and Rudnick et al. (2017, submitted) using similarly defined samples for direct comparison. Table 2 provides some information on these samples.

3 VISUAL CLASSIFICATION OF STRUCTURAL DISTURBANCES

To complement the information provided by the galaxies’ morphological Hubble types (Desai et al. 2007), in this paper we qualitatively analyse galaxy ‘structure’ by studying the detailed distribution of galaxy light. For this purpose, we use the terms ‘asymmetry’ to refer to visible departures from a symmetric light profile, and ‘disturbance’ to indicate our assessment of whether the cause of that deviation is internal or external in origin. Therefore, a galaxy may have a combination of ‘asymmetry’ and ‘disturbance’ properties. For instance, a galaxy may be symmetric and undisturbed; another may be internally asymmetric but undisturbed (e.g. an otherwise symmetric spiral galaxy with a prominent HII region); a third

one may be asymmetric due to an external distortion (e.g., gravitational interaction). To clarify all these possible categories, Figure 1 gives a graphical representation of the classification scheme, described below.

This classification was carried out by visually inspecting *HST* images of all the galaxies in our sample taken in the *I*-band (corresponding, approximately, to the rest-frame *B*-band). Three of the authors (KK, AAS, MEG) performed independent classifications of every galaxy. Note that these classifications were carried out blindly, without knowledge of the cluster membership of the galaxies, their redshifts or their morphology type.

3.1 Visual asymmetry class

As a first step in the classification, we separate galaxies into two distinct classes, ‘symmetric’ and ‘asymmetric’. This is done by visually identifying asymmetric features in the galaxies images as possible indicators of structural disturbances. Explicitly, we classified galaxies as ‘asymmetric’ if they possess asymmetric features, and ‘symmetric’ in the absence of them.

3.2 Visual disturbance class

For those galaxies with visual asymmetry, we further designed a classification scheme, independent of morphological type, to identify the probable cause of the disturbance. Figure 1 gives a graphical representation of the classification scheme, described below.

- **Internal Asymmetry (iA)** : The galaxies classified under this category showed distinct visual asymmetry due to features like prominent star-forming regions/knots in the galaxy. Further, these asymmetries showed no clear evidence of any form of external processes which may be acting on the target galaxy. These galaxies are assigned a non-zero asymmetry but no disturbance index and constitute only $\sim 7\%$ of the total sample. However, note that such internal asymmetries may well still be the result of external causes like mergers (Bournaud, Duc & Emsellem 2008) or ram-pressure stripping events (Poggianti et al. 2016), even though these may not be apparent.

- **Galaxy interaction (i/I)** : Galaxies in this class showed features indicating interactions with a companion galaxy. Lowercase “i” denotes ‘weak interaction’, while uppercase “I” indicates ‘strong interaction’, as judged by the classifier.

- **Tidal interaction (t/T)** : Galaxies in this class displayed tidal features (e.g. a tail of stripped material extending outside the galaxy) but with no obvious sign of an interacting neighbour. As before, lowercase/uppercase letters are used to indicate the strength of the features.

- **Mergers (m/M)** : We identified ongoing galaxy mergers based on distinct asymmetric merging signatures. Minor or major mergers were identified through a visual assessment of the stellar mass ratios involved. Galaxies appearing as a single distorted merger remnant or possessing clear galaxy cores of similar brightness were classified as major mergers (M). Galaxies seen merging with a smaller galaxy were identified as minor mergers (m). Our classifications are informed by the visual appearance of merging galaxies in simulations, and experience of classifying mergers in STAGES (Gray et al. 2009) and EDiCS.

- **Chaotic/Undefined systems (C/X)** : The final class contained a small number of galaxies (less than 1% of the total sample) displaying structures that were chaotic or could not be associated with any of the categories above.

Final classifications

Symmetric galaxies were assigned an index of ‘0’, whereas asymmetric galaxies were indexed as ‘a’/‘A’, with the lower/upper case of the index denoting an assessment of the strength (weak/strong) of the asymmetric features. Asymmetric galaxies were then assigned a disturbance class label according to the schema described above, with the lower/upper case of the index denoting the mild/strong nature of the external features. To determine the strength of the visual classification (ie weak/strong), individual indices of ‘0’ were given a weight of 0 while lower/upper case indices were given a weight of ‘1’ and ‘2’ respectively.

Since three independent classifiers classified each galaxy, the final combined classification for asymmetry and disturbance was determined by majority vote (independent of the index case). The final classification was then associated with the summed weights of the contributing indices. If all the three classifiers disagreed, the final classification was selected at random from the three votes. The strength of classification in this case would be the weight of the randomly selected classification index. In a small number of cases where a classifier was not confident in the assessment, the individual contribution was downweighted to 0.5.

Also note one further subtlety in our classification scheme. A subset of galaxies with smooth early-type morphologies (asymmetry = ‘0’) nevertheless were identified on the balance of probability as having a disturbance class (minor interaction, ‘i’) based on the presence of a very close neighbour. These ‘0&i’ galaxies represent possible dry merger candidates, where a merger may be ongoing but the visual signatures are short-lived due to an absence of gas in the galaxies (Bell et al. 2006).

Table 3 gives the fractions of galaxies in each disturbance class in the cluster and field environment with respect to the entire sample. We use the Wilson (1927) binomial confidence interval to compute the 1σ uncertainty in the fractions δf_i

$$\hat{f}_i \pm \delta \hat{f}_i = \frac{N_i + \kappa^2/2}{N_{\text{tot}} + \kappa^2} \pm \frac{\kappa\sqrt{N_{\text{tot}}}}{N_{\text{tot}} + \kappa^2} \sqrt{f_i(1 - f_i) + \frac{\kappa^2}{4N_{\text{tot}}}}, \quad (1)$$

where $f_i = N_i/N_{\text{tot}}$, and κ is the $100(1 - \alpha/2)$ th percentile of a standard normal distribution (α being the error percentile corresponding to the 1σ level (refer also to Brown, Cai & DasGupta 2001)). These fractions will be discussed in Section 6. Note that even if $N_i = 0$, the estimated value of \hat{f}_i is not necessarily 0.

4 QUANTITATIVE STRUCTURE

In addition to our *qualitative* assessment of galaxy asymmetry and disturbance, we also further explore *quantitative* measurements of galaxy structure. Specifically, we extract structural information from the galaxy residuals after a smooth surface brightness profile is removed. Although originally intending to identify minor mergers, Hoyos et al. (2012) show that measuring structural parameters of residuals of galaxies is a good way of determining disturbances in galaxy structure that are otherwise faint to detect visually but are observable over a longer timescale.

4.1 Constructing galaxy residual images

The galaxy residual images required for this analysis were obtained using the data pipeline GALAPAGOS (Galaxy Analysis over Large Area: Parameter Assessment by GALFITting Objects from SEXTRACTOR; Barden et al. 2012). All galaxies from the ten *HST*

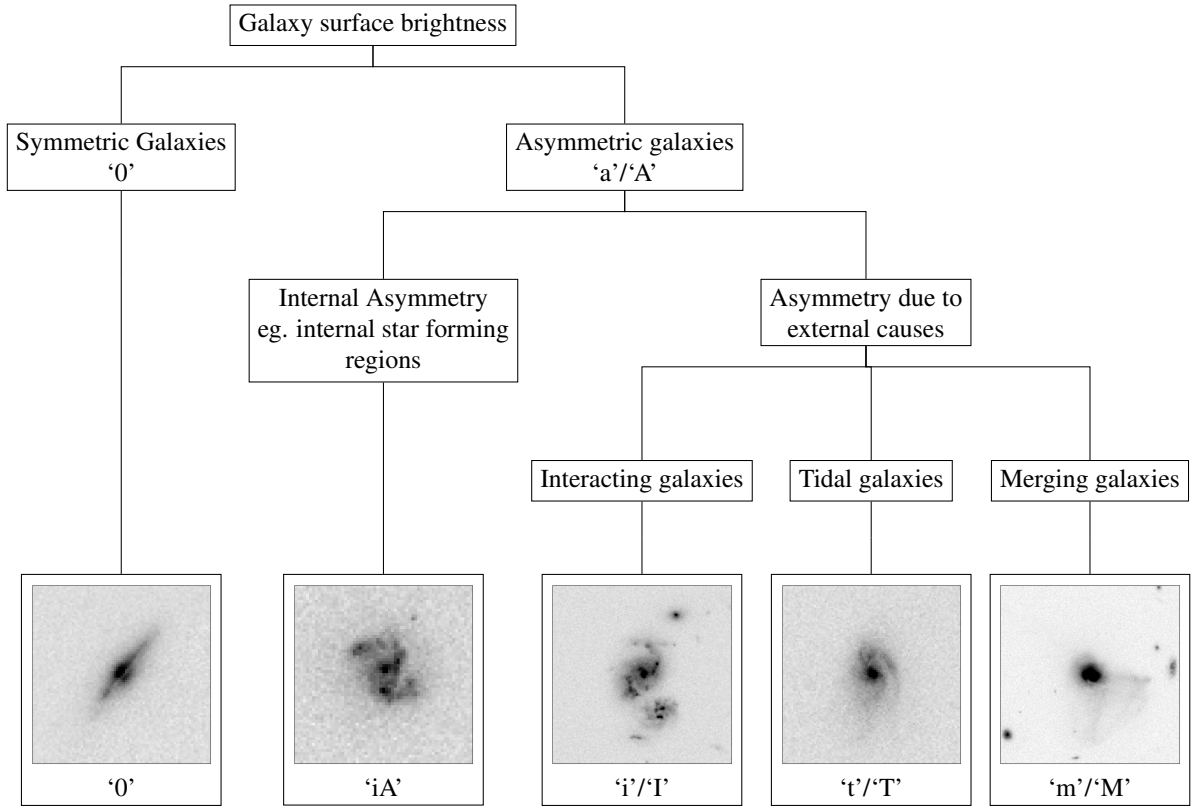


Figure 1. Graphical representation of our classification scheme for identifying structural disturbances. We use a two-stage process: first visually identifying galaxies with some form of asymmetry in their surface brightness distribution, then further refining that classification based on an evaluation of the probable cause of the disturbance (whether internal or external in origin). The images are *HST* thumbnails of representative galaxies from the sample identified in each class. Additionally, a small number of galaxies classified as ‘Chaotic’ (C) or ‘Undefined’ (X), and are not included in this diagram. Please refer to Section 3 for details regarding classification scheme.

Table 3. The relative fractions for galaxies identified as undisturbed, internally asymmetric (possessing asymmetry but with no obvious external cause), interacting galaxies, tidal galaxies and galaxies experiencing an ongoing merger, for a fixed morphology in cluster and field environment. Refer to Section 6 for detailed discussion.

Morphology	Environment	Undisturbed	Internally asymmetric	Interacting	Tidal	Merger
		(0)	(iA)	(i/I)	(t/T)	(m/M)
Ellipticals (E)	Cluster	0.79±0.04	0.01±0.01	0.17±0.04	0.02±0.01	0.02±0.01
	Field	0.64±0.08	0.08±0.05	0.14±0.06	0.11±0.05	0.08±0.05
Lenticulars (S0)	Cluster	0.93±0.04	0.01±0.01	0.07±0.04	0.01±0.01	0.01±0.01
	Field	0.85±0.11	0.05±0.05	0.15±0.11	0.05±0.05	0.05±0.05
Spirals (Sp)	Cluster	0.35±0.03	0.25±0.03	0.18±0.03	0.09±0.02	0.11±0.02
	Field	0.36±0.05	0.22±0.04	0.20±0.04	0.11±0.03	0.11±0.03
Irregulars (Irr)	Cluster	0.03±0.03	0.38±0.12	0.15±0.08	0.09±0.06	0.32±0.11
	Field	0.02±0.02	0.21±0.09	0.12±0.07	0.21±0.09	0.40±0.11

I-band mosaics were detected using SEXTRACTOR, and corresponding image stamps were created by GALAPAGOS. These image stamps were fitted with a 2D Sérsic light profile (Sérsic & de Córdoba. Observatorio Astronómico 1968) using GALFIT (Peng et al. 2002, 2010a), which resulted in generation of galaxy residual stamp images after the Sérsic model was subtracted. Kelkar et al. (2015) contains further details of the fitting method. These residual images were used to compute quantitative ‘Asymmetry’ (A_{res}) and a measurement of the signal remaining after subtracting the Sérsic model (residual flux fraction, ‘RFF’).

4.2 Asymmetry in residual images (A_{res})

Using the CAS (Concentration, Asymmetry, Clumpiness; Bershady, Jangren & Conselice 2000) system, we define the asymmetry ‘ A_{res} ’ in the galaxy residual image to measure the extent of residual light under a 180 degree rotation around a point that minimizes the asymmetry of the galaxy image. It is defined as:

$$A_{\text{res}} = \left(\frac{\sum_{i,j} |I_{i,j} - I_{i,j}^{180}|}{\sum_{i,j} |I_{i,j}|} \right) - \left(\frac{\sum_{i,j} |B_{i,j} - B_{i,j}^{180}|}{\sum_{i,j} |I_{i,j}|} \right), \quad (2)$$

Here $I_{i,j}$ represents the flux at pixel (i,j) in the galaxy residual image whereas $I_{i,j}^{180}$ represents the same image rotated through 180 degrees. The second term in the equation accounts for the background contribution. We construct a background noise image to compute the second term using the EDiSCS noise images for the *HST* ACS mosaics. As with the construction of the residual images, associated noise images were cut out for individual galaxies with the same dimensions as the residual images.

As a first step, these noise stamp images were multiplied with the exposure time corresponding to the region in the mosaic (Refer to §2). This modified image was then multiplied by a white noise image with $\sigma = 1$. The resultant image is a good representation of the background noise. Both the terms in the above equation are computed over an aperture defined by constructing an ellipse whose semimajor axis is the radius of Kron aperture² and are minimised independently. We implement a slightly modified method for minimising these terms, deviating from the original recipe described in Conselice, Bershady & Jangren (2000). We allow the centre of rotation to lie at a maximum of 3 pixels in radius from the SEXTRACTOR defined centre over a grid of predefined points 1 pixel apart. The main advantage of this new method is that the pixel values are not interpolated under 180-degree rotation due to the choice of integral rotation centres. Moreover, one could think of this method computing global rotational asymmetry, and hence reducing the computation time as compared to the original method. The possible values that A_{res} can take ranges from 0 to 2.

4.3 Residual flux fraction (RFF)

The second quantitative diagnostic we use is the Residual Flux fraction (Hoyos et al. 2011, 2012), which gives the fraction of signal

² In this paper, we use the definition of radius of the ‘‘Kron aperture’’: $2.2r_1$, where r_1 is the first moment of the light distribution (Bertin & Arnouts 1996). This corresponds to the semimajor axis for an elliptical light distribution.

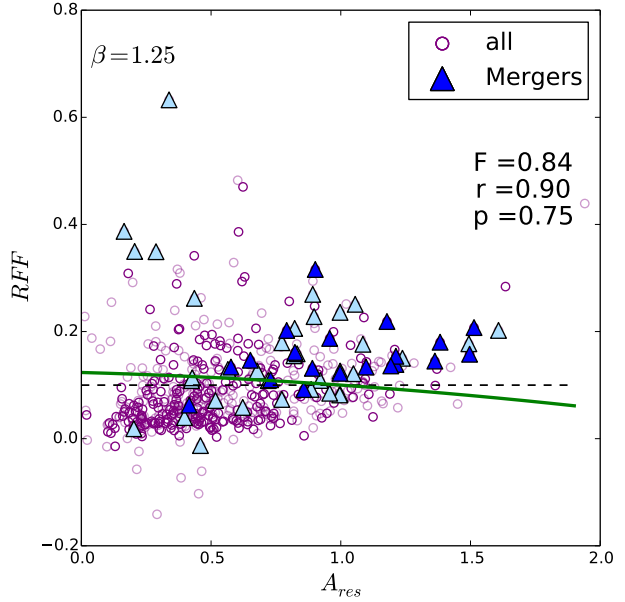


Figure 2. The $RFF - A_{\text{res}}$ plane with the statistical best border (green) for galaxies classified as mergers, constructed using a mass-complete sample. The lighter coloured triangles and circles denote low-mass galaxies excluded from the analysis. The dashed line indicates the initial approximation used to compute the border. The r and p values illustrate the completeness and purity of the division: 90% of mergers from the training sample lie above the border (true positives) while 75% of non-mergers lie below the border (true negatives). Note that the final border remains nearly horizontal, indicating that RFF alone provides a good indication of merger status for our sample.

contained in the residual image of the galaxy that cannot be explained by the background fluctuations. It is defined as:

$$RFF = \frac{\sum_{i,j} |I_{i,j} - I_{i,j}^{\text{GALFIT}}| - 0.8 \times \sum_{i,j} \sigma_{i,j}^{\text{bkg}}}{\sum_{i,j} I_{i,j}^{\text{GALFIT}}}, \quad (3)$$

where $I_{i,j}$ represents the flux at pixel (i,j) in the galaxy image, while $I_{i,j}^{\text{GALFIT}}$ is the model created by GALFIT. The *rms* of the background is $\sigma_{i,j}^{\text{bkg}}$. As discussed previously, we use the same galaxy residual images for computation of RFF over the Kron aperture. The factor of 0.8 enables the expectation value of RFF for purely Gaussian noise error image of constant variance to be 0.0.

4.4 Defining galaxy structure

Hoyos et al. (2012) show that A_{res} and RFF are capable of automatically detecting structural disturbances in galaxies when used together. Using a training sample of visually identified galaxy mergers from the low redshift STAGES field (Gray et al. 2009), Hoyos et al. (2012) show that these mergers occupy a specific region on the RFF vs A_{res} plane. This enables a statistical division of the parent sample into two sub-populations: one containing mergers with some contamination by non-merging galaxies, and the other almost devoid of any merging galaxies (a powerful null test).

We use the same technique on our mass-complete sample to identify a subsample of structurally disturbed galaxies that we can

compare with our qualitative identifications. We examine the RFF vs A_{res} distribution for the entire population of galaxies in our sample of morphologically classified galaxies with spectroscopic information. We divide our sample by defining a separating border as a second order polynomial of RFF in terms of A_{res} and separates visually identified mergers from non-mergers.

The statistical quality of the two populations is determined by the F -score, F_β (Rijsbergen 1979) given by

$$F_\beta = \frac{(1 + \beta^2) \times p \times r}{(\beta^2 \times p + r)}, \quad (4)$$

where ‘ r ’ denotes the sensitivity or completeness of the method, and ‘ p ’ denote specificity or the true negative rate. The factor β is a control parameter which determines the relative importance of r and p . In this work, we have used $\beta = 1.25$, to be consistent with Hoyos et al. (2012). This border is then optimized such that it maximizes the F -score.

In order to apply the F -score maximization for detection of galaxy structure, we use a training sample of galaxies classified visually as mergers from our parent sample to calculate r and p . Figure 2 shows both populations for the mass-complete sample, with the separating border represented by the green solid line. The galaxies above the solid green line denote the positive detections of galaxies being mergers, with the merger training sample retrieved with a high completeness ($\sim 90\%$) and a contamination of $\sim 25\%$ by galaxies not classified as mergers. Refer to Hoyos et al. (2012), for the detailed method.

We note that including low-mass galaxies ($\log M_*/M_\odot < 10.6$) does not change the border significantly. We are able to separate the merger subsample from the parent sample, albeit with lower completeness. For comparison, the galaxies with masses below the mass completeness are overplotted in light blue in Figure 2. It is clear that this method gives a clean sample of non-merging galaxies. Comparing to Hoyos et al. (2012), we see a significant flattening of the border separating the mergers. This can be attributed to the lower S/N of galaxies at intermediate redshifts, as compared to the local sample of STAGES galaxies used in Hoyos et al. (2012). This is also reflected in the range of RFF and A_{res} values. However, the important outcome of this analysis is that while it is possible to separate regular galaxies from the disturbed galaxies using these two non-parametric measures, it is the RFF that is the most significant discriminator of galaxy structure in our sample. Thus, RFF gives a measure of ‘roughness’ in galaxy structure.

Comparing the border determined using the visually classified mergers to the distribution of galaxies showing disturbances due to other external causes, we see that this technique is consistent in separating structurally disturbed galaxies. Figure 3 shows the merging, tidal and interacting galaxies on the RFF vs A_{res} plane. The F -score, r and p for the tidal and interacting galaxies is computed using the border determined for the merger training subset. Although the location is comparable for merging and tidal galaxies on this plane, we find interacting galaxies extend below the separating line in RFF . Therefore, in accordance with the classification scheme, we separate the ‘true’ interacting galaxies from the visually symmetric interacting galaxies (open yellow triangles), despite the presence of a companion. We note that, as expected, the symmetric interacting galaxies (dry merger candidates, or ‘0&i’) are the objects populating the region below the separating border in the RFF vs A_{res} plane.

5 LINK BETWEEN THE QUALITATIVE AND QUANTITATIVE STRUCTURE

We next connect the quantitative measures of galaxy structure with our visual classification scheme, recalling the need to control for morphology. Using the CAS system, Conselice (2003) evaluate the relative variation in the ‘Asymmetry’ of galaxies when we consider their morphologies. Galaxies with early-type morphologies displayed lower asymmetries compared to late-type, star forming or disky galaxies. We do find consistent results when comparing A_{res} of galaxies with mild/strong visual asymmetry for a fixed morphology (Figure 4). We see that galaxies with elliptical/lenticular morphology are generally visually symmetric (‘0’) with very low structural asymmetry in their residuals. The spiral galaxies, however, show a distinct separation in structural asymmetry in the residuals for mildly and strongly visually asymmetric galaxies, confirming that visual and structural asymmetry are strongly correlated. The irregular galaxy sample is small, but as expected they are all asymmetric with typically high RFF and A_{res} values.

We next consider the variation of quantitative measures of structure with the visually determined causes of disruption. Figure 5 shows the distribution of RFF and A_{res} for galaxies disrupted due to different mechanisms. If we consider only the RFF of galaxies, we find that RFF alone is not able to distinguish the tidal, merging and internally asymmetric galaxies, indicating that RFF is sensitive to the degree of disturbance rather than the cause of the disturbance. This result is also graphically demonstrated when comparing the best border for galaxies in different disturbance classes in Figure 3. Additionally, the subclass of symmetric interacting galaxies (‘0&I’) seem to have RFF distributions similar to galaxies with regular morphologies, although the distribution for the true interacting galaxies lies in between.

The lower panel of Figure 5 shows the distribution of A_{res} for different disturbance classes. Interestingly, a significant stratification is seen in the distribution of A_{res} for different disturbance classes, with undisturbed galaxies having a low A_{res} and mergers showing extreme values of A_{res} .

We conclude that RFF is able to separate galaxies with disturbed structure from those with regular undisturbed structure, but has little discriminatory power to differentiate between the different types (or causes) of such disturbances. On the other hand, A_{res} is more sensitive to the different types (or causes) of structural disturbance in the galaxies. In simple terms, RFF can be used as a measure of the degree of structural disturbance, while A_{res} provides information on the cause of it. Or, more precisely, a combination of both parameters can be used to provide information on both the degree and the cause of galaxy deviations from symmetry.

6 STRUCTURE AND STAR FORMATION VS GLOBAL ENVIRONMENT

6.1 Effect of global environment on galaxy disturbances

This analysis uses the spectroscopic sample with visual classifications to compare the properties of galaxies as a function of global environment (e.g., cluster vs. field) rather than a more continuous measure of local environment. That will be the object of a subsequent paper (Kelkar et al. 2017, in prep).

In Section 2.1 we described a full redshift-controlled field sample together with a mass-complete subsample. The full sample has the advantage of being significantly larger, but it suffers from incompleteness for galaxies with $\log M_*/M_\odot < 10.6$. Neverthe-

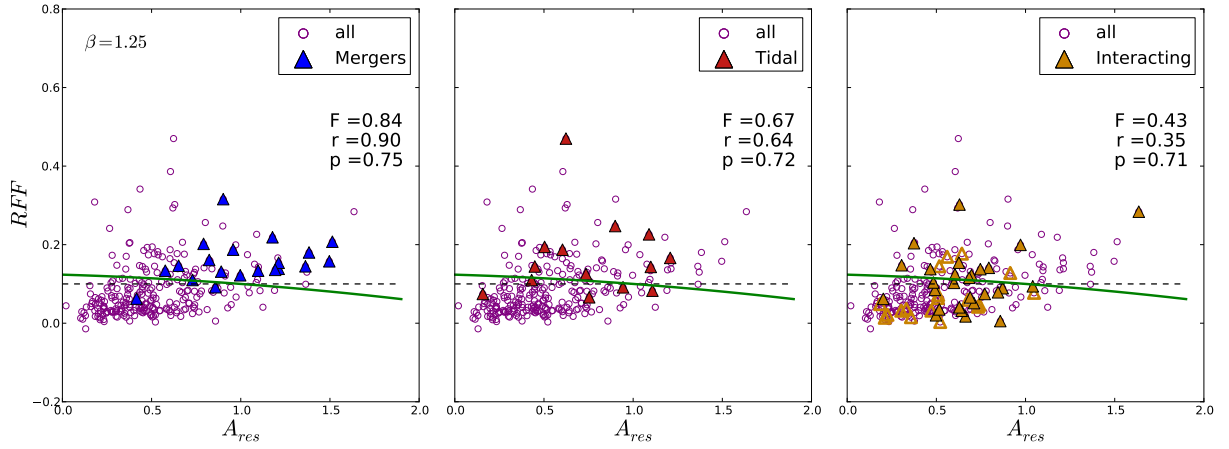


Figure 3. Comparison of the $RFF - A_{res}$ plane for all externally disturbed classes of galaxies: mergers (left), tidal (centre), and interacting (right), using the mass-complete sample. As in Figure 2, the dashed and solid lines indicate the initial approximation and the final border computed using the merger class of galaxies (blue). The F -score, r and p values for each class of galaxies are computed using this border. The open triangles in the right panel denote the subclass of interacting galaxies nevertheless classified as ‘symmetric’ according to our classification scheme (discussed in §4.4).

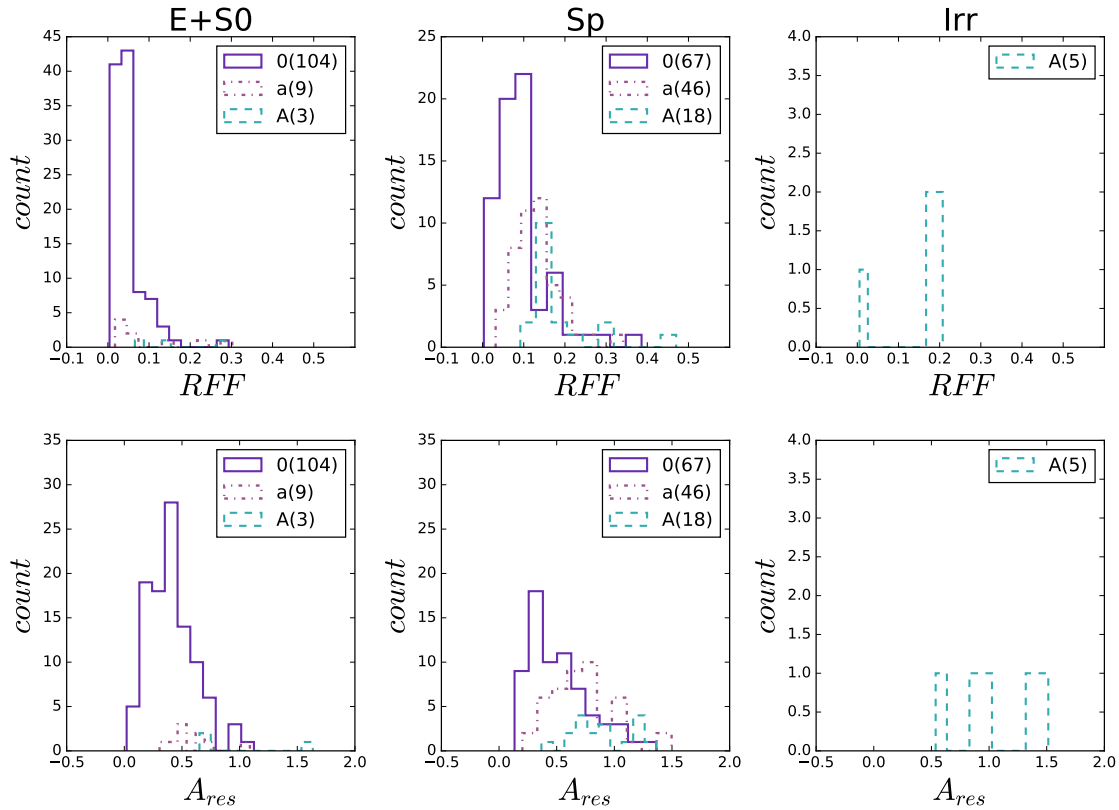


Figure 4. Separating quantitative measurements of structure by visual asymmetry. The histograms show the distributions of RFF and A_{res} for visually symmetric (0), mild (a) and strongly asymmetric (A) galaxies at fixed morphology. Early-type galaxies (E+S0) show little quantitative or qualitative evidence for asymmetry or disturbance. Both top and bottom panels for spiral galaxies (middle) clearly show a separation in RFF and A_{res} , with higher values corresponding to the strongest visual asymmetries.

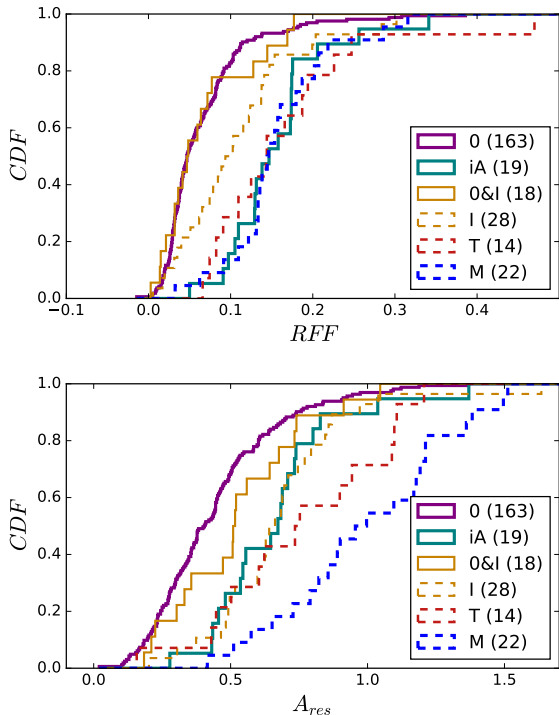


Figure 5. Distributions of two quantitative measurements of structure by visual disturbance class. Here we show the cumulative distributions of RFF (top) and A_{res} (bottom) for galaxies separated according to the degree and source of any visual disturbance. The distributions are labelled according to the physical processes introduced in §3 and Table 3. However, for the interacting galaxies, we have plotted the separate distributions for the subclass of symmetric interacting galaxies (‘0&I’) whereas ‘I’ denotes the main class of interacting galaxies displaying obvious visual asymmetry. Note that while RFF clearly separates symmetrical galaxies (‘0’, ‘0&I’) from the remaining classes, A_{res} has further discriminatory power according to the *cause* of any asymmetry, with internal asymmetries (‘iA’) and interacting galaxies (‘I’) having some of the lowest values and mergers (‘M’) having the largest.

less, because the selection and the observation of cluster and field galaxies over the relevant redshift range is identical, the incompleteness should affect field and cluster galaxies equally. With this in mind, when carrying out comparisons between the properties of cluster and field galaxies it should be safe to use the full redshift-controlled sample. Nevertheless, we will carry out a parallel analysis using the smaller mass-complete subsample to test whether our conclusions depend on the exact sample that we use. In general, we find that the conclusions described below for the full sample are consistent with the ones we obtain for the mass-complete sample within the statistical uncertainties. Further, to remove additional effects brought in by the fact that galaxy morphology depends strongly on environment (Dressler 1984; Treu et al. 2003; Desai et al. 2007), we look at the disturbance content of galaxies in clusters and field at fixed morphology (Table 3). We find that the fractions of galaxies classified visually as interacting, tidal and merging do not seem to depend on the environment.

6.2 Distribution of galaxy disturbances and star formation as a function of global environment

As discussed in the introduction, the internal and external physical mechanisms in various galaxy environments are responsible for the transformation of galaxy structure as well as star formation. Although disentangling the relative importance of these processes is difficult, quenching in the star formation of galaxies is observed in dense environments (Balogh et al. 2007; Haines et al. 2013; Kovač et al. 2014). With the aim of studying the possible links between the quenching of star formation and the morphological change in galaxies, we next look at the star formation properties of structurally disturbed galaxies.

It was found by Wuyts et al. (2007) and Williams et al. (2009) that galaxies show a strong bimodality on the rest-frame ($U-V$) vs ($V-J$) colour-colour space, with the actively star-forming galaxies following a diagonal path and the quiescent galaxies populating upper-left region on this space (see also Wolf, Gray & Meisenheimer 2005; Labbé et al. 2005). Moreover, the ($U-V$) vs ($V-J$) plane is more robust to separate the dusty star-forming galaxies from the passive galaxies, as compared to the single colour selection. Therefore, we construct a rest-frame ($U-V$) vs ($V-J$) colour plot (UVJ hereafter) to distinguish the passive and star-forming population (Figure 6; see also Patel et al. 2012). The UVJ plot shows that the low-mass galaxies ($\log M_*/M_\odot \leq 10.6$) are bluer in colour, as expected from the existing correlations between mass, metallicity, star-formation rate and dust extinction (Lara-López et al. 2010).

The empirical selection criteria for passive galaxies, as introduced by Williams et al. (2009), highlights the observed bimodal distribution of galaxies on the UVJ plane at low- z , and the subsequent weakening at high- z . Figure 6 shows such a distribution for galaxies in our sample with different morphologies. The boundary separating star-forming and passive galaxies in the UVJ plane is somewhat arbitrary, and Williams et al. (2009) found that this boundary is weakly redshift dependent. It will also depend on the exact photometric bands used in the observations. In Figure 6 we show the boundaries selected by Williams et al. (2009) for two redshift ranges, $0.5 < z < 1$ and $z > 1$. Given the redshift of our galaxies, the $0.5 < z < 1$ boundary should be, in principle, more appropriate. However, we notice that the $z > 1$ boundary seems to do a much better job at separating the bimodal colour distribution than the lower redshift one, in particular if we take into account the location of galaxies with different morphologies. A density-mapping analysis corroborates this visual impression, revealing that galaxies with early-type morphologies populate the upper left region of the UVJ plot, as defined by the $z > 1$ boundary, while the late-type spiral and irregular galaxies occupy the diagonal sequence, and the separation is significantly better with this boundary than with the $0.5 < z < 1$ one. We concluded that for our specific dataset, the $z > 1$ boundary is better at separating star-forming from non-star-forming galaxies. Explicitly, we use the boundary defined by

$$\begin{cases} (U-V) \geq 1.3 & (5) \\ (U-V) \geq 0.88 * (V-J) + 0.49 & (6) \\ (V-J) \leq 1.6 & (7) \end{cases}$$

to separate passive non-star-forming galaxies (inside the upper-left box) from star-forming ones.

Figure 7 shows the fraction of passive and star forming galaxies of each morphology type in various structural disturbance

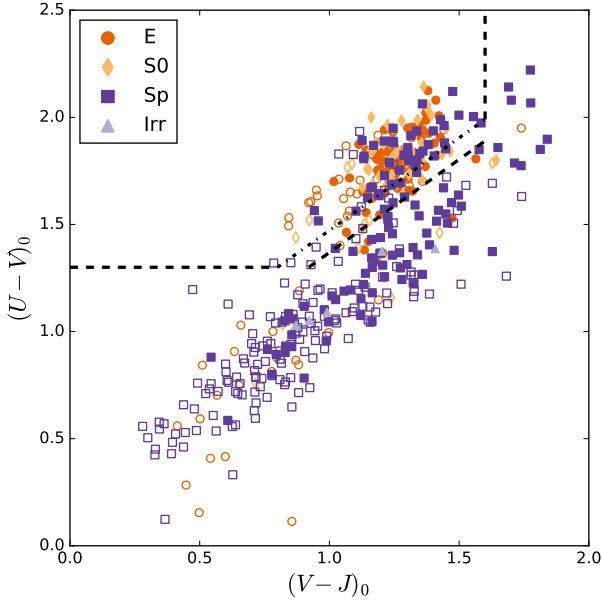


Figure 6. Rest-frame UVJ colour plot for the ellipticals (circle/orange), lenticulars (diamond/yellow), spirals (squares/violet), and irregulars (triangles/light violet). The galaxies are defined as passive and star-forming according to the boundaries of Williams et al. (2009) for the two redshift bins: $0.5 < z < 1$ (dashdot) and $z > 1$ (dashed). The empty symbols denote galaxies with masses below the mass completeness limit.

classes, and global environments. It is evident from each of the four panels that galaxies with early-type morphology are visually smoother compared to the galaxies of late-type/irregular morphology, which is expected from the distinguishing physical properties of these two subpopulations.

Most spirals show asymmetries, and for those, a flat distribution of spirals across the disturbance classes (most of which are external in origin) is observed. Furthermore, in each disturbance class nearly all are star-forming, indicating a strong correlation of star formation with external causes of structural disturbances. We also note a relatively higher fraction of cluster star-forming spirals displaying tidal features as compared to the field. These spirals could be the potential candidates with ‘jellyfish’ morphology (Ebeling, Stephenson & Edge 2014; Poggianti et al. 2016). Likewise, all of the irregulars are both disturbed according to their stellar distribution, and star-forming according to their photometry. We can, thus, say that external processes lead to star formation in galaxies irrespective of their morphology. However, the star formation can also be triggered internally in galaxies. In general, it is seen that the passive population in the sample – irrespective of their morphology – tend to have lower RFF and lower A_{res} , and hence are structurally smoother and symmetric. This correlation, however, seems to be independent of the global environment.

6.3 A population of smooth passive spirals in clusters

We make particular note of those spiral galaxies that are simultaneously classified as visually smooth/undisturbed and passive. Figure 7 shows that most are found to reside in clusters, with the majority ($> 70\%$) of these having stellar masses greater than the mass completeness limit, both in cluster and field environment. This ob-

servation agrees with the findings from works such Poggianti et al. (1999); Wolf et al. (2009); Cantale et al. (2016), Rodriguez del Piño et al. (2016, MNRAS, in press), who both find a significant fraction of passive spirals in the cluster environment that may represent a key transition population undergoing slow environmental quenching (See also Bamford et al. 2009; Masters et al. 2010). Most recently, Hoyos et al. (2016) reported that optically passive spiral galaxies in clusters, at a given mass, tend to have lower star formation rates and smoother structure as compared to the galaxies in field. This result is particularly relevant here because these authors used quantitative structural measurements similar to the ones we present in this paper.

To test whether quantitative measurements of galaxy disturbance support the findings based on our visual diagnostics, we present in Figures 8 and 9 the rest-frame UVJ diagram colour-coded with respect to RFF and A_{res} , for cluster and field galaxies. Complementing Figure 7, both panels in Figure 8 show that these passive undisturbed spirals have lower RFF , indicating a smoother structure. This is further enhanced in Figure 9, where we see that passive spirals in clusters are much more symmetric with low A_{res} . This observation combines the result from Figures 5 and 7 demonstrating the external nature of structural disturbances for the majority of the asymmetric spirals, and the different behaviour of A_{res} in the different disturbance classes.

We use two-sample Kolmogorov-Smirnov (K-S) tests to check whether the RFF and A_{res} distributions for these passive spirals, and the regular undisturbed spirals are statistically similar. Figure 10 compares the RFF and A_{res} distributions for passive spirals and regular undisturbed spirals, both in cluster and field environments. The KS tests yields probabilities of 5.3×10^{-4} and 0.02 for these distributions to be the same for cluster and field galaxies respectively. This emphasises the fact that passive spirals tend to show statistically smaller RFF values and are therefore smoother than star-forming ones irrespective of their global environment. However, the distributions of A_{res} for passive and star-forming spirals appear to be only marginally different in clusters (K-S test probability of 0.03), while the small number statistics prevent a robust comparison for field spirals.

These results reinforce our findings from Figure 7, implying that the effect of the cluster environment on the spiral galaxy population is to increase the fraction of passive smooth spiral galaxies without destroying their spiral morphology. This would signify that spirals on entering clusters become structurally smooth due to the quenching of their star formation followed later by morphological transformation, perhaps into S0s. This implies that the mechanisms ultimately responsible for the quenching of these galaxies star formation in clusters must be reasonably gentle, affecting primarily the gas while leaving the galaxies’ stellar structure largely unchanged. These galaxies become smoother due to the suppression of the star formation itself, since ‘rough’ structures such as HII regions would disappear (see, e.g., Hoyos et al. 2016). Gas-driven mechanisms such as ram-pressure stripping are therefore strongly favoured. These conclusions are in good agreement with the findings of Bösch et al. (2013) based on observation of the lower redshift STAGES field (Gray et al. 2009), which show that red spirals display distinct asymmetries in their gas rotation curves, and are therefore preferentially experiencing ram-pressure stripping, as compared to normal spiral galaxies.

Complementary conclusions were obtained by Cantale et al. (2016, see their Figure 10) using the UVJ colours of disks in the EDiSCS dataset. These authors find that $\sim 50\%$ of cluster spirals have redder disks than their field counterparts at fixed morphology,

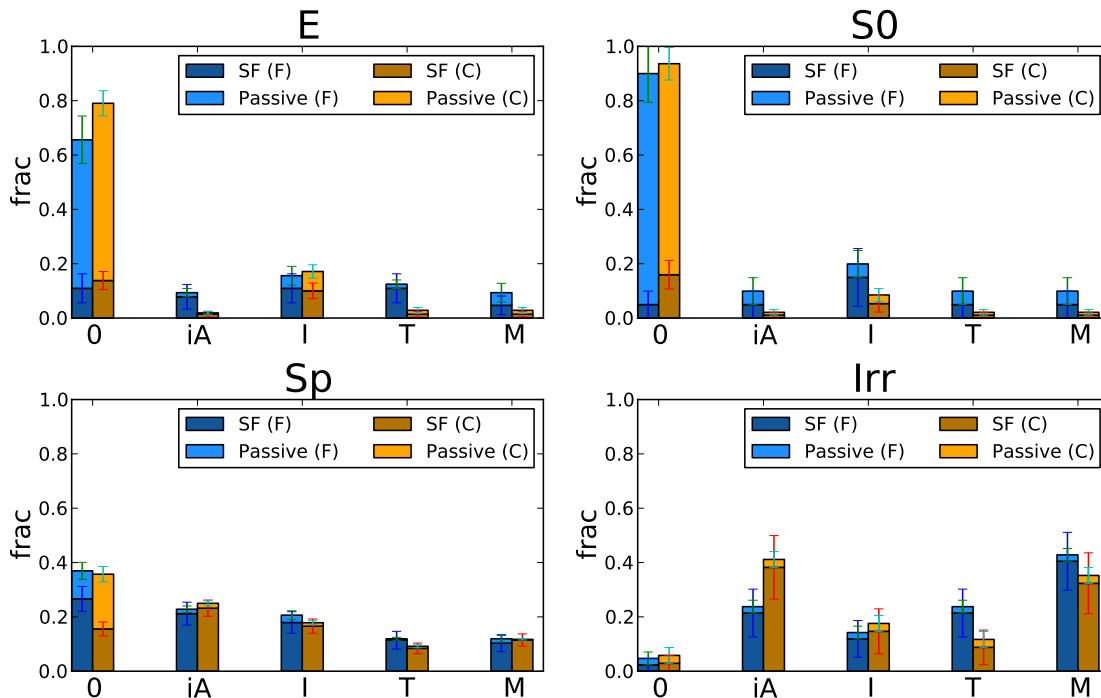


Figure 7. Visual galaxy structure at fixed morphology according to the global environment. Each panel shows the fractions of galaxies in different disturbance classes for a given morphology, in the field (blue/left column) and cluster (orange/right column) environments. The dark shaded region in each bar shows the fraction of star-forming galaxies in that class of morphology, disturbance class, and environment. In both cluster and field environments, less than half of all spiral galaxies are visually symmetric ('0'), while for asymmetric galaxies the causes of the disturbance are roughly equally distributed between internal causes ('iA'), interactions ('I'), tidal forces ('T'), and mergers ('M'). Note also that for symmetric spirals, a marginally significantly higher fraction (2.3σ) in cluster environments are passive than in the field. Conversely, passive spirals are only found in the visually symmetric class.

but they also find evidence that spiral galaxies must have continued forming stars for a significant period of time after their accretion into the clusters, getting quenched thereafter on a timescale of a few Gyrs.

6.4 A small population of star-forming cluster S0s

Turning our attention to lenticular (S0) galaxies, Figure 7 indicates that, as expected, the vast majority of these galaxies are symmetric and passive both in clusters and in the field. However, although the numbers are small and the statistical uncertainties very large, there seems to be some marginal evidence suggesting the presence of an excess of star-forming S0 galaxies in clusters with respect to the field. Some of these star-forming S0s are asymmetric, showing signs of perturbation (interactions, mergers and tidal features), but there seems to be also a population of symmetric star-forming S0s in clusters which is absent in the field. Specifically, we do not find a single symmetric undisturbed star-forming S0 in the field, although the expectation value of their fraction shown in Figure 7 is not 0 (cf. Equation 1). Although the undisturbed lenticulars have a wide spectrum of stellar masses in all environments, we note that the majority ($> 80\%$) of the symmetric star-forming cluster lenticulars have relatively low stellar masses that are below the completeness limit. It is therefore not impossible, albeit unlikely, that these galaxies may have been missed preferentially in the field. If that is not the case, this result supports the findings of Johnston, Aragón-Salamanca & Merrifield (2014), suggesting that in the pu-

tative transformation of spirals into S0s in clusters, a final episode of star formation takes place in the central regions (bulges) of these galaxies after the disk star formation has ceased. In this scenario, the gas is removed from the disk of the spirals, while some gas remains in (and/or is channelled to) the bulge, where this final gasp of star formation takes place. This process probably requires an external cause and it may therefore be cluster-specific. That could explain why this final episode of star formation is not observed in undisturbed field S0s, where other formation mechanisms may need to be invoked.

7 CONCLUSIONS

In this paper we present a detailed analysis of the structure of a sample of field and cluster galaxies at intermediate redshift ($0.4 < z < 0.8$) using Hubble Space Telescope images from the ESO Distant Cluster Survey (EDisCS) which approximately sample the B -band in the rest-frame of the galaxies. We combine this structural information with extensive photometric and spectroscopic data to study the links between galaxy structure and other internal properties such as mass, morphology and star-formation history, and how these are affected by the global environment where the galaxies live.

We have analysed the galaxies' structure following two parallel methods. In the first one, we visually inspected the galaxies' *HST* images and classified them into symmetric and asymmetric;

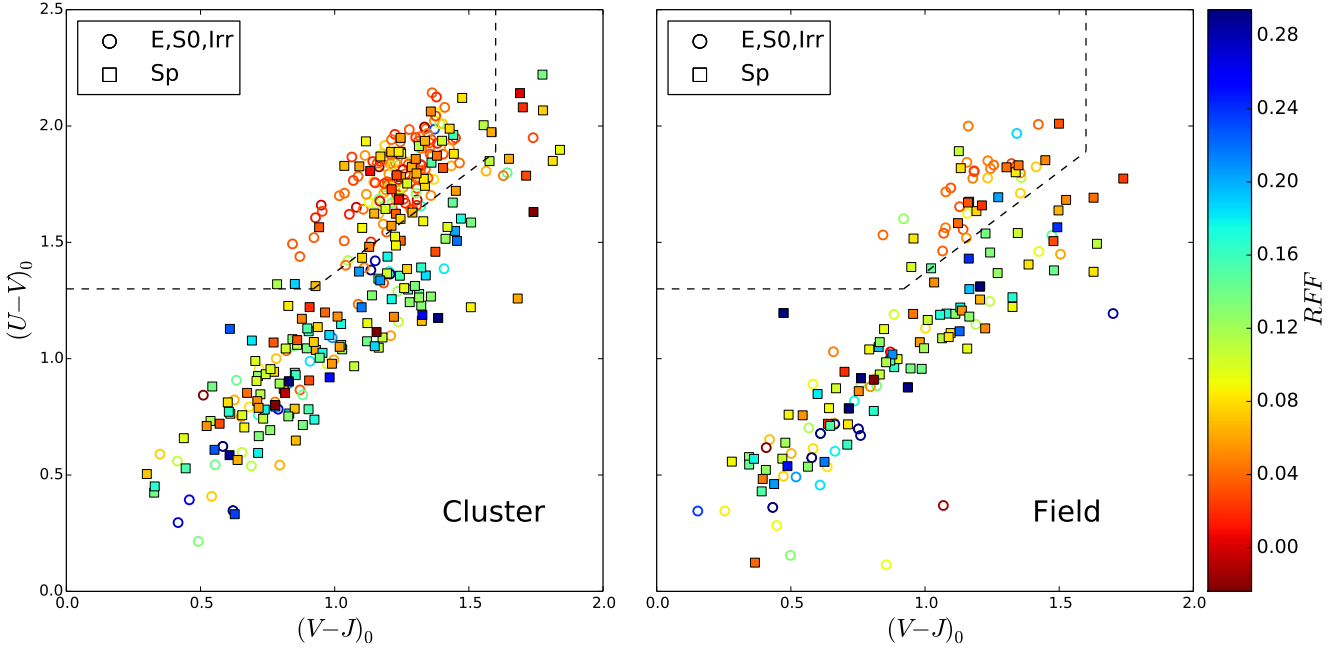


Figure 8. The UVJ plot is colour-coded according to RFF values for the cluster (left panel) and field (right panel) galaxies: redder colours indicate smoother, undisturbed galaxies while bluer colours denote ‘roughness’, irrespective of galaxy morphology or global environment. As in Figure 6, the dashed lines show the selection boundaries for passive galaxies. Complementing Figure 7, both panels show that the passive undisturbed spirals have lower RFF , indicating a smoother structure.

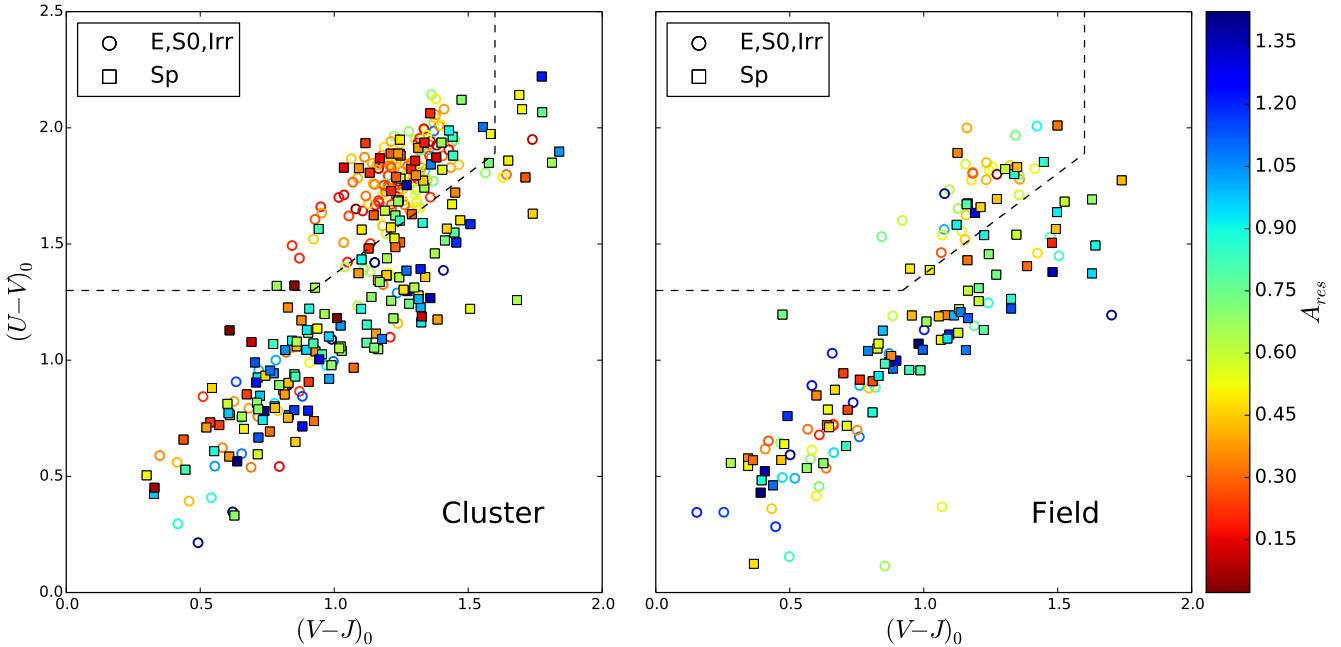


Figure 9. Similar to Figure 8, the UVJ plot is here colour-coded according to A_{res} for cluster (left panel) and field (right panel) galaxies. Star-forming galaxies are consistently found to be more quantitatively asymmetric than passive galaxies irrespective of morphology or global environment. Moreover, complementing Figure 8, the passive spirals in clusters are found to be more symmetric with low A_{res} .

the asymmetric class was further divided into subclasses that try to identify the likely cause of the asymmetry (internal asymmetry, galaxy-galaxy interactions, tidal interactions, and mergers). The second method uses quantitative non-parametric measurements of the galaxies’ deviation from a smooth symmetric light distribution.

An elliptical Sérsic model is first fitted to the galaxies’ *HST* images, and the residuals are then quantified using the RFF (Residual Flux Fraction, measuring the fractional contribution of the residuals to the total galaxy light, taking into account the noise), and A_{res} (the

asymmetry of the residual light distribution). The main conclusions of this structural analysis are:

- The qualitative (visual classification) and quantitative (RFF and A_{res}) assessments of galaxy structure provide consistent and complementary information.
- RFF is able to separate galaxies with disturbed structure from those with regular undisturbed structure, but has little discriminatory power to differentiate between the different types (or causes) of such disturbances. On the other hand, A_{res} is more sensitive to the different types (or causes) of structural disturbance in the galaxies. A combination of both parameters can therefore be used to provide information on both the degree and the cause of galaxy deviations from symmetry.

We then link this structural information with the galaxies' masses, morphologies and star-formation histories, and conclude that:

- As expected, the vast majority of elliptical and S0 galaxies are smooth and symmetric, while all irregular galaxies are “rough” and asymmetric. Statistically, spiral galaxies tend to have higher values of RFF and A_{res} than early-type galaxies.
- Over 60% of all spiral galaxies are visually classified as showing some degree of asymmetry. Of these, about one third exhibit asymmetry of internal origin (due, e.g., to the presence of large star-forming regions), while the rest show signs of galaxy-galaxy interactions, tidal interactions or mergers in comparable proportions.
- In agreement with the results of Hoyos et al. (2016), we find that RFF correlates strongly with the star-formation activity of the galaxies: star-forming galaxies tend to have much “rougher” structures.

Finally, the global environment (cluster vs. field) of the galaxies is taken into consideration, and we find that:

- At fixed morphology, there are no significant differences in the distribution of the disturbance classes of cluster and field galaxies.
- About 40% of all the spiral galaxies are classified as symmetric and undisturbed both in clusters and in the field. However, the fraction of these that are passive (i.e., non-starforming) is twice as large in clusters than in the field: about half of the cluster symmetric spirals are passive, vs. only one quarter in the field (with a significance of 2.3σ). These passive spirals are not only visually symmetric, but also quantitatively smoother (i.e., have smaller RFF values) than star-forming ones.
- While nearly all lenticular galaxies are visually symmetric and undisturbed both in clusters and in the field, *all* the field ones are passive, while nearly $\sim 20\%$ in the clusters are star-forming.

These results have significant implications for the evolution of spiral galaxies falling onto clusters and their subsequent transformation. Spirals entering clusters become structurally smooth (and red) due to the quenching of their star formation, but retain their spiral morphology for a while. The morphological evolution follows later, transforming them, probably, into S0s. The mechanism(s) ultimately responsible for the quenching of these galaxies star formation in clusters must primarily affect the gas while leaving the galaxies stellar structure largely unchanged. Gas-driven mechanisms such as ram-pressure stripping (where the disk gas is partially or totally stripped) and/or starvation/strangulation (where the gas supply is truncated), are therefore favoured. These conclusions are in good agreement with the findings of Bösch et al. (2013) based on observation of the lower redshift STAGES field (Gray et al. 2009), which show that red spirals display distinct asymmetries

in their gas rotation curves, and are therefore preferentially experiencing ram-pressure stripping, as compared to normal spiral galaxies. Similar conclusions were obtained by Jaffé et al. (2011) for EDisCS galaxies. This general scenario also agrees with observations indicating a rapid build-up of red-sequence galaxies earlier than the build up of early-type galaxies as seen in clusters (Desai et al. 2007; De Lucia et al. 2007; Wolf et al. 2009; Rudnick et al. 2009, 2012; Cerulo et al. 2016).

At a more speculative level, our analysis also provides some clues on the putative transformation of spirals into S0s. The star-forming S0s we find in the clusters (but not the field) could be the descendants of the spiral galaxies experiencing a last episode of star formation before becoming S0s, supporting the findings of Johnston, Aragón-Salamanca & Merrifield (2014). These authors suggest that when spirals transform into S0s in clusters, a final episode of star formation takes place in the central regions (bulges) of these galaxies after the disk star formation has ceased. In this scenario, the gas is removed from the disk of the spirals, while some gas remains in (and/or is channelled to) the bulge, where this final gasp of star formation takes place. This process probably requires an external cause (e.g., ram pressure) and it may not work in the field. This could explain why this final episode of star formation is not observed in undisturbed field S0s, where other formation mechanisms may need to be invoked.

Focusing on the general question of “nature” vs. “nurture” in galaxy evolution, it is now clear that the processes leading to the cessation of star formation depend both on internal properties (e.g., stellar mass) and environment, with the dominant quenching mechanisms being environmentally-driven or mass-driven for different mass ranges, cosmic epochs, and environments (Peng et al. 2010b; Thomas et al. 2010). Studies at lower (Baldry et al. 2006; Wetzel, Tinker & Conroy 2012) and higher redshifts (Muzzin et al. 2012) show that the quiescent fraction is correlated with both stellar mass and environment, and this relationship is maintained even at $z > 1$ (Quadri et al. 2012; Cooke et al. 2016; Hatch et al. 2016). With the importance of environmental quenching increasing with cosmic time and decreasing with stellar mass, our analysis is particularly relevant because we explore the intermediate mass and redshift regimes, where both stellar mass and environment probably play significant roles in shutting down the star formation. In addition, focusing on differences in the internal galaxy structure at fixed morphology has allowed us to uncover subtle environmental effects that broader-brush studies had missed.

However, the work published here does not provide sufficient details on the possible environmental mechanisms at play because we have only considered global environments such as clusters and the field, disregarding more localised effects. This will be the focus of Kelkar et al. (2017, in prep.) where we use tools like the projected phase-space diagram to constrain the detailed environmental history of the cluster galaxies. Moreover, studying directly the timescales associated with the quenching of star formation will provide very valuable complementary information (Wolf et al. 2017, in prep.).

ACKNOWLEDGMENTS

Based on observations made with the NAS/ESA *Hubble Space Telescope*, obtained at the Space Telescope Science Institute, which is operated by the Association of Universities for Research in Astronomy, Inc., under NASA contract NAS 5-26555. These observations are associated with proposal 9476. Support for this proposal

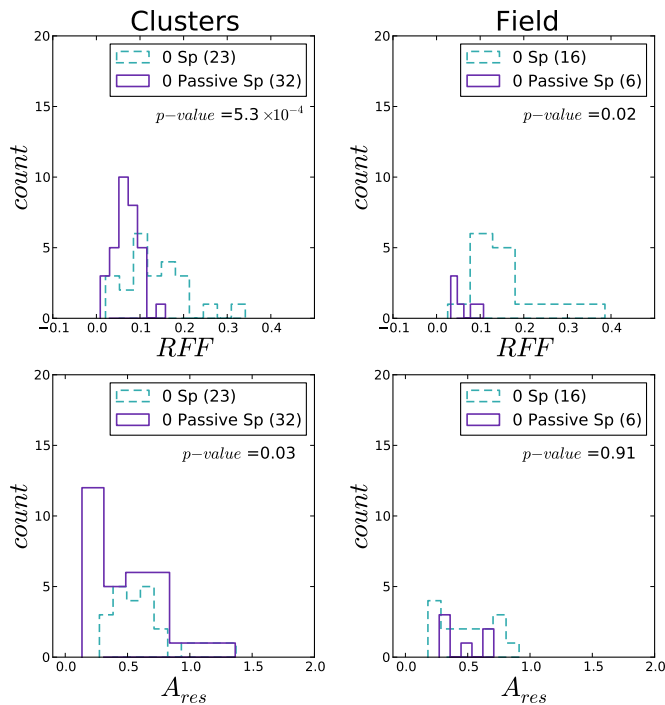


Figure 10. RFF and A_{res} distributions for spiral galaxies in cluster (left panel) and field (right panel) environments. The solid purple histograms show the subset of passive symmetric spirals, as discussed in §6.3. The inset ‘ p -values’ give the probability from two sample K-S test, showing that in addition to being visually symmetric, the cluster passive spirals are quantitatively ‘smoother’.

was provided by NASA through grant from the Space Telescope Science Institute.

Based on observations obtained at the ESO Very Large Telescope (VLT) as a part of the Large Programme 166.A-0162

We acknowledge the EDisCS team for providing a unique dataset, and useful comments on the work presented in this paper. We also thank Yara Jaffé for valuable discussions regarding the visual classifications. We would also like to thank the referee for useful comments and feedback which helped in making the contents of this paper better. GHR acknowledges the support of NASA grant *HST*-AR-12152.001-A, NSF grants 1211358 and 1517815, the support of an ESO visiting fellowship, and the hospitality of the Max Planck Institute for Astronomy, the Max Planck Institute for Extraterrestrial Physics, and the Hamburg Observatory. GHR also acknowledges the support of a Alexander von Humboldt Foundation Fellowship for experienced researchers. GHR recognizes the support of the International Space Sciences Institute for their workshop support.

REFERENCES

Baldry I. K., Balogh M. L., Bower R. G., Glazebrook K., Nichol R. C., Bamford S. P., Budavari T., 2006, *MNRAS*, 373, 469
 Balogh M. L. et al., 2007, *MNRAS*, 374, 1169
 Bamford S. P. et al., 2009, *MNRAS*, 393, 1324
 Barden M., Häußler B., Peng C. Y., McIntosh D. H., Guo Y., 2012, *MNRAS*, 422, 449
 Barnes J. E., Hernquist L., 1992, *ARA&A*, 30, 705
 Barnes J. E., Hernquist L., 1996, *ApJ*, 471, 115

Bell E. F. et al., 2006, *ApJ*, 640, 241
 Bershadsky M. A., Jangren A., Conselice C. J., 2000, *AJ*, 119, 2645
 Bertin E., Arnouts S., 1996, *A&AS*, 117, 393
 Boquien M. et al., 2009, *AJ*, 137, 4561
 Bösch B. et al., 2013, *A&A*, 549, A142
 Bournaud F., Duc P.-A., Emsellem E., 2008, *MNRAS*, 389, L8
 Brown L. D., Cai T. T., DasGupta A., 2001, *Stat. Sci.*, 16, 101
 Butcher H., Oemler, Jr. A., 1984, *ApJ*, 285, 426
 Cantale N. et al., 2016, *A&A*, 589, A82
 Cerulo P. et al., 2016, *MNRAS*, 457, 2209
 Conselice C. J., 2003, *ApJS*, 147, 1
 Conselice C. J., Bershadsky M. A., Jangren A., 2000, *ApJ*, 529, 886
 Cooke E. A. et al., 2016, *ApJ*, 816, 83
 Cooper M. C. et al., 2012, *MNRAS*, 419, 3018
 De Lucia G., Kauffmann G., White S. D. M., 2004, *MNRAS*, 349, 1101
 De Lucia G. et al., 2007, *MNRAS*, 374, 809
 De Lucia G., Poggianti B. M., Halliday C., Milvang-Jensen B., Noll S., Smail I., Zaritsky D., 2009, *MNRAS*, 400, 68
 Desai V. et al., 2007, *ApJ*, 660, 1151
 Dressler A., 1980, *ApJ*, 236, 351
 Dressler A., 1984, *ARA&A*, 22, 185
 Dressler A. et al., 1997, *ApJ*, 490, 577
 Duc P.-A., Brinks E., Wink J. E., Mirabel I. F., 1997, *A&A*, 326, 537
 Ebeling H., Stephenson L. N., Edge A. C., 2014, *ApJL*, 781, L40
 Elbaz D., Cesarsky C. J., 2003, *Science*, 300, 270
 Fasano G., Poggianti B. M., Couch W. J., Bettoni D., Kjærgaard P., Moles M., 2000, *ApJ*, 542, 673
 Ferguson H. C., Dickinson M., Williams R., 2000, *ARA&A*, 38, 667
 Finn R. A. et al., 2005, *ApJ*, 630, 206
 Freeman P. E., Izbicki R., Lee A. B., Newman J. A., Conselice C. J., Koekemoer A. M., Lotz J. M., Mozena M., 2013, *MNRAS*, 434, 282
 Fumagalli M., Fossati M., Hau G. K. T., Gavazzi G., Bower R., Sun M., Boselli A., 2014, *MNRAS*, 445, 4335
 Gallazzi A. et al., 2009, *ApJ*, 690, 1883
 Gavazzi G., Fumagalli M., Cucciati O., Boselli A., 2010, *A&A*, 517, A73
 Gonzalez A. H., Zaritsky D., Dalcanton J. J., Nelson A., 2001, *ApJS*, 137, 117
 Gray M. E. et al., 2009, *MNRAS*, 393, 1275
 Gray M. E., Wolf C., Meisenheimer K., Taylor A., Dye S., Borch A., Kleinheinrich M., 2004, *MNRAS*, 347, L73
 Gunn J. E., Gott, III J. R., 1972, *ApJ*, 176, 1
 Haines C. P. et al., 2013, *ApJ*, 775, 126
 Halliday C. et al., 2004, *A&A*, 427, 397
 Hashimoto Y., Oemler, Jr. A., Lin H., Tucker D. L., 1998, *ApJ*, 499, 589
 Hatch N. A., Muldrew S. I., Cooke E. A., Hartley W. G., Almaini O., Simpson C. J., Conselice C. J., 2016, *MNRAS*, 459, 387
 Hoyos C. et al., 2012, *MNRAS*, 419, 2703
 Hoyos C., Aragón-Salamanca A., Gray M. E., Wolf C., Maltby D. T., Bell E. F., Böhm A., Jogee S., 2016, *MNRAS*, 455, 295
 Hoyos C. et al., 2011, *MNRAS*, 411, 2439
 Jaffé Y. L. et al., 2011, *MNRAS*, 417, 1996
 Jaffé Y. L., Smith R., Candlish G. N., Poggianti B. M., Sheen Y.-K., Verheijen M. A. W., 2015, *MNRAS*, 448, 1715
 Johnson O. et al., 2006, *MNRAS*, 371, 1777
 Johnston E. J., Aragón-Salamanca A., Merrifield M. R., 2014, *MNRAS*, 441, 333

- Kartaltepe J. S. et al., 2012, *ApJ*, 757, 23
- Kauffmann G., White S. D. M., Heckman T. M., M enard B., Brinchmann J., Charlot S., Tremonti C., Brinkmann J., 2004, *MNRAS*, 353, 713
- Kelkar K., Arag on-Salamanca A., Gray M. E., Maltby D., Vulcani B., De Lucia G., Poggianti B. M., Zaritsky D., 2015, *MNRAS*, 450, 1246
- Kenney J. D. P., van Gorkom J. H., Vollmer B., 2004, *AJ*, 127, 3361
- Koekemoer A. M., Fruchter A. S., Hook R. N., Hack W., 2003, in *HST Calibration Workshop : Hubble after the Installation of the ACS and the NICMOS Cooling System*, Arribas S., Koekemoer A., Whitmore B., eds., p. 337
- Kova c K. et al., 2014, *MNRAS*, 438, 717
- Kroupa P., 2001, *MNRAS*, 322, 231
- Labb e I. et al., 2005, *ApJL*, 624, L81
- Lara-L opez M. A., Bongiovanni A., Cepa J., P erez Garc ıa A. M., S anchez-Portal M., Casta neda H. O., Fern andez Lorenzo M., Povi c M., 2010, *A&A*, 519, A31
- Larson R. B., Tinsley B. M., Caldwell C. N., 1980, *ApJ*, 237, 692
- Lewis I. et al., 2002, *MNRAS*, 334, 673
- Lotz J. M., Jonsson P., Cox T. J., Primack J. R., 2008, *MNRAS*, 391, 1137
- Lotz J. M., Jonsson P., Cox T. J., Primack J. R., 2010, *MNRAS*, 404, 575
- Lotz J. M., Primack J., Madau P., 2004, *AJ*, 128, 163
- Madau P., 1997, in *American Institute of Physics Conference Series*, Vol. 393, American Institute of Physics Conference Series, Holt S. S., Mundy L. G., eds., pp. 481–490
- Masters K. L. et al., 2010, *MNRAS*, 405, 783
- Merluzzi P. et al., 2013, *MNRAS*, 429, 1747
- Milvang-Jensen B. et al., 2008, *A&A*, 482, 419
- Moore B., Katz N., Lake G., Dressler A., Oemler A., 1996, *Nature*, 379, 613
- Muzzin A. et al., 2012, *ApJ*, 746, 188
- Patel S. G., Holden B. P., Kelson D. D., Franx M., van der Wel A., Illingworth G. D., 2012, *ApJL*, 748, L27
- Peng C. Y., Ho L. C., Impey C. D., Rix H.-W., 2002, *AJ*, 124, 266
- Peng C. Y., Ho L. C., Impey C. D., Rix H.-W., 2010a, *AJ*, 139, 2097
- Peng Y.-j. et al., 2010b, *ApJ*, 721, 193
- Poggianti B. M. et al., 2009, *ApJ*, 693, 112
- Poggianti B. M. et al., 2016, *AJ*, 151, 78
- Poggianti B. M., Smail I., Dressler A., Couch W. J., Barger A. J., Butcher H., Ellis R. S., Oemler, Jr. A., 1999, *ApJ*, 518, 576
- Poggianti B. M. et al., 2006, *ApJ*, 642, 188
- Quadri R. F., Williams R. J., Franx M., Hildebrandt H., 2012, *ApJ*, 744, 88
- Rijsbergen C. J. V., 1979, *Information Retrieval*, 2nd edn. Butterworth-Heinemann, Newton, MA, USA
- Rudnick G. et al., 2009, *ApJ*, 700, 1559
- Rudnick G. H., Tran K.-V., Papovich C., Momcheva I., Willmer C., 2012, *ApJ*, 755, 14
- Schrabback T. et al., 2010, *A&A*, 516, A63
- S ersic J., de C ordoba. Observatorio Astron mico U. N., 1968, *Atlas de galaxias australes*. Observatorio Astronomico, Universidad Nacional de Cordoba
- Simard L. et al., 2009, *A&A*, 508, 1141
- Sobral D., Best P. N., Smail I., Geach J. E., Cirasuolo M., Garn T., Dalton G. B., 2011, *MNRAS*, 411, 675
- Thomas D., Maraston C., Schawinski K., Sarzi M., Silk J., 2010, *MNRAS*, 404, 1775
- Tremonti C. A. et al., 2004, *ApJ*, 613, 898
- Treu T., Ellis R. S., Kneib J.-P., Dressler A., Smail I., Czoske O., Oemler A., Natarajan P., 2003, *ApJ*, 591, 53
- van den Bosch F. C., Aquino D., Yang X., Mo H. J., Pasquali A., McIntosh D. H., Weinmann S. M., Kang X., 2008, *MNRAS*, 387, 79
- Vulcani B., Poggianti B. M., Finn R. A., Rudnick G., Desai V., Bamford S., 2010, *ApJL*, 710, L1
- Wetzel A. R., Tinker J. L., Conroy C., 2012, *MNRAS*, 424, 232
- White S. D. M. et al., 2005, *A&A*, 444, 365
- Williams R. J., Quadri R. F., Franx M., van Dokkum P., Labb e I., 2009, *ApJ*, 691, 1879
- Wilson E. B., 1927, *J. Am. Stat. Assoc.*, 22, 209
- Wolf C. et al., 2009, *MNRAS*, 393, 1302
- Wolf C., Gray M. E., Meisenheimer K., 2005, *A&A*, 443, 435
- Woo J. et al., 2013, *MNRAS*, 428, 3306
- Wuyts S. et al., 2007, *ApJ*, 655, 51

This paper has been typeset from a $\text{\TeX}/\text{\LaTeX}$ file prepared by the author.